


 Cite this: *RSC Adv.*, 2021, 11, 5537

Turning over on sticky balls: preparation and catalytic studies of surface-functionalized TiO₂ nanoparticles†

 Sven A. Freimann,^{ID} Alessandro Prescimone,^{ID} Catherine E. Housecroft^{ID} and Edwin C. Constable^{ID}*

We have investigated the reactivity of rhodium(III) complex-functionalized TiO₂ nanoparticles and demonstrate a proof-of-principle study of their catalytic activity in an alcohol oxidation carried out under aqueous conditions water in air. TiO₂ nanoparticles (NPs) have been treated with (4-((2,2':6',2''-terpyridin)-4'-yl)phenyl)phosphonic acid, **1**, to give the functionalized NPs (**1**)@TiO₂. Reaction between (**1**)@TiO₂ NPs and either RhCl₃·3H₂O or [Rh₂(μ-OAc)₄(H₂O)₂] produced the rhodium(III) complex-functionalized NPs Rh(**1**)₂@TiO₂. The functionalized NPs were characterized using thermogravimetric analysis (TGA), matrix-assisted laser desorption ionization (MALDI) mass spectrometry, ¹H NMR and FT-IR spectroscopies; the single crystal structures of [Rh(**1**)₂][NO₃]₃·1.25[H₃O][NO₃]·2.75H₂O and of a phosphonate ester derivative were determined. ¹H NMR spectroscopy was used to follow the reaction kinetics and to assess the recyclability of the NP-supported catalyst. The catalytic activity of the Rh(**1**)₂@TiO₂ NPs was compared to that of a homogeneous system containing [Rh(**1**)₂]³⁺, confirming that no catalytic activity was lost upon surface-binding. Rh(**1**)₂@TiO₂ NPs were able to withstand reaction temperatures of up to 100 °C for 24 days without degradation.

 Received 2nd November 2020
 Accepted 22nd January 2021

DOI: 10.1039/d0ra09319j

rsc.li/rsc-advances

Introduction

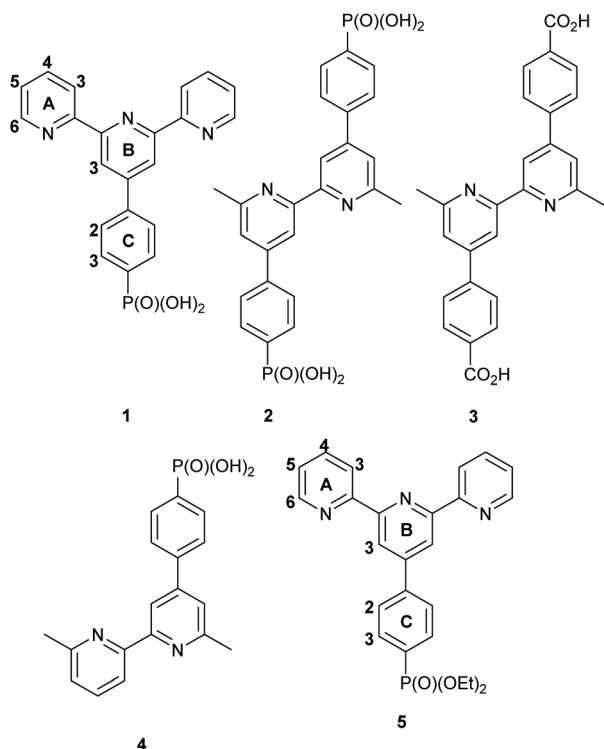
In general, catalytic processes are categorized as homogeneous or heterogeneous. Homogeneous catalysts have the advantage that all of the catalytic centres are potentially active, whereas in heterogeneous catalysts only the surface catalytic sites of solid phases are active as interior sites are inactive.¹ With solid phase heterogeneous catalysts, reaction only takes place at the interface rather than in the bulk of the reactant volume. On the other hand, it is often easier to separate the products of heterogeneous catalysis from the spent catalyst than in the case of homogeneous catalysis.^{2,3} Heterogeneous catalysts also have significant benefits in terms of catalyst recovery, a feature gaining increasing environmental and economic importance.

Nanoparticle (NP) immobilized catalysts have the potential of bridging the gap between these two extreme types of catalysis. Firstly, NPs exhibit greater surface-to-volume ratios than bulk heterogeneous catalysts and the catalyst loading capacity, catalytic activity and turnover will be enhanced, in particular the catalytic site-to-volume ratio will be high.⁴ Secondly, the ability to disperse NPs in solution gives some of the benefits of homogeneous catalysts. NP-supported catalysts have attracted great interest and offer already outstanding diversity and range in the chemical and pharmaceutical field.⁵⁻⁷

The advantages of NP supported catalysts have been demonstrated for a number of key reactions. For the Suzuki–Miyaura coupling reaction, palladium-decorated benzene-1,2-diamine-functionalized Fe₃O₄/SiO₂ magnetic NPs were utilized and showed excellent yields within short reaction times.¹ Gold NP-supported ruthenium catalysts have been used for ring-opening metathesis polymerization of bicyclo[2.2.1]hept-2-ene (norbornene) and show a higher activity than the unsupported counterparts.⁸ Nickel NP-based catalysts were active in the steam–reformation reaction of methane showing excellent conversion, H₂ selectivity and thermal stability.⁹ These reactions often make use of valuable and rare elements that cannot be efficiently recovered in the case of homogeneous catalysis. Recyclability of a catalyst is essential and conventional heterogeneous catalysts have the benefit that they can be easily recovered compared to homogeneous catalysts. Dispersed NPs are more challenging to separate than conventional

Department of Chemistry, University of Basel, BPR 1096, Mattenstrasse 24a, CH-4058 Basel, Switzerland. E-mail: edwin.constable@unibas.ch

† Electronic supplementary information (ESI) available: Fig. S1–S2: Mass and ¹H NMR spectra of [Rh(**1**)₂]Cl₃; Fig. S3: Precipitation of AgCl from [Rh(**1**)₂]Cl₃; Fig. S4–S13: Mass, ¹H NMR and 2D NMR spectra of [Rh(**1**)₂]Cl₃; Fig. S14–S21: ¹H NMR, 2D NMR, solution absorption spectra and ORTEP representation of [Rh(**5**)₂][PF₆]₃; Fig. S22–S27: solid-state IR and absorption spectra, TGA curves and Mass spectra of NP-[Rh(**1**)₂]³⁺; Fig. S28 and S29: ¹H NMR and solid-state IR comparison spectra, Fig. S30 and S31 TGA curves from commercial NPs and (**1**)@TiO₂ NPs, Fig. S32–S35: Mass and solid-state IR spectra of [Rh(**5**)₂][PF₆]₃; Fig. S36: ¹H NMR spectrum of [Rh(**1**)₂]Cl₃. CCDC 2040345 and 2025772. For ESI and crystallographic data in CIF or other electronic format see DOI: 10.1039/d0ra09319j



Scheme 1 Structures of compounds 1–5.

heterogeneous catalysts but the recoverability is still greater than with most homogenous catalysts. Furthermore, NPs can be modified to boost recoverability by introducing additional characteristics such as magnetic properties.

The benefits of NPs are well-established in the oxidation of alcohols, a key step in the synthesis of many organic compounds.⁷ The transformation of alcohols to aldehydes, ketones or carboxylic acids generally needs stoichiometric quantities of hazardous, environmentally damaging and toxic oxidants such as chromium trioxide, dichromate, permanganate and chromic acid.¹⁰

We have recently demonstrated¹⁴ the functionalization of TiO₂ NPs with ligands **1**, **2**, **3** and **4** (see Scheme 1) which bind to the metal oxide surface through their phosphonate or phosphonic acid groups and we were interested in investigating the activity of complexes incorporating these surface-bound ligands. We report here the assembly of surface-bound rhodium complexes of ligand **1** related to [Rh₂Cl₂(μ-OAc)(tpy)₂]⁺ reported by Wang *et al.*¹² We compare the catalytic behaviour of functionalized TiO₂ NPs to the homogeneous catalytic performance of [Rh(**1**)₂]Cl₃ and [Rh(**5**)₂][PF₆]₃. We have also investigated the kinetics of these reactions, the recyclability of the NP catalyst over 5 cycles, and the influence of the concentration of base on the catalytic activity of the functionalized nanoparticles.

Experimental

General

Instrumentation details are given in the ESI.†

Ligands **1** and **5** (Scheme 1),¹³ were prepared according to the literature and their spectroscopic data matched those

previously reported. TiO₂ NP activation and functionalization with ligand **1** were carried out according to our previously published procedure.¹¹ MALDI mass spectra were recorded using α-cyano-4-hydroxycinnamic acid (CHCA) as the matrix.

[Rh₂(μ-OAc)₄(H₂O)₂] and *rac*-(1*R*)-1-phenylethanol were purchased from Acros Organics and Sigma Aldrich respectively. RhCl₃·3H₂O was purchased from Johnson Matthey, Materials Technology UK. Microwave vials (5 mL and 20 mL) were from Biotage and were selected depending on the required solvent volume.

TiO₂ NPs (AEROXIDE TiO₂ P25) were purchased from Evonik Industries. The spherical NPs have an average radius of 10.5 nm (ref. 14) and an average surface area-to-volume ratio of 28%. The number of equivalents of NPs is defined as 0.28 × the total number of TiO₂ formula equivalents in the mass given, *i.e.* the effective surface concentration of TiO₂.¹¹ Similarly, when clarifying equivalents or mmol of functionalized NPs, it refers to the estimated amount of ligand or complex bound to the surface.

Activation of commercial P25 TiO₂ NPs

The commercial NPs were activated as previously described¹¹ but the procedure was scaled up as follows. Commercial P25 TiO₂ NPs (2.00 g) were dispersed by sonication for 15 min in dilute aqueous HNO₃ (30 mL, 3 M). The mixture was then stirred for 30 min. The NPs were separated from the acid by centrifugation (10 min, 9000 rpm) and washed once with milliQ water (30 mL). The NPs were again dispersed in milliQ water (20 mL) through sonication for 10 min and the suspension was then stirred overnight. The NPs were separated by centrifugation (10 min, 9000 rpm) and washed with milliQ water (2 × 20 mL). The activated NPs (1.85 g) were stored in a sealed vial under N₂ after drying over high vacuum.

Preparation of (1)@TiO₂ NPs

The functionalization was done as previously reported¹¹ but the procedure was scaled up as follows. Ligand **1** (29.2 mg, 0.075 mmol, 1 eq.) and milliQ water (18 mL) were added to a microwave vial and dispersed through sonication for 1 min. Activated TiO₂ NPs (660 mg, 30.8 TiO₂ eq.) were added to the solution and the mixture was dispersed with sonication for 10 min. The microwave vial was sealed and the reaction mixture heated for 3 h at 130 °C in the microwave reactor. The (1)@TiO₂ NPs were separated from the solvent by centrifugation (30 min, 9000 rpm) after cooling to room temperature. The white (1)@TiO₂ NPs (674 mg) were stored in a sealed vial under N₂ after drying under high vacuum. For NMR measurements, (1)@TiO₂ NPs (5–10 mg) were dispersed in 500 μL D₂O in an NMR tube.

Attempted synthesis of [Rh₂(μ-OAc)(1)₂]Cl

Compound **1** (81.8 mg, 0.210 mmol, 2 eq.) was dispersed with NaCl (61.4 mg, 1.05 mmol, 10 eq.) through sonication for 10 min in ethanol (5 mL). [Rh₂(μ-OAc)₄(H₂O)₂] (50.2 mg, 0.105 mmol, 1 eq.) was added. Argon was bubbled through the suspension for 5 minutes while stirring. The suspension was stirred under argon at 80 °C for 18 h. The reaction mixture was allowed to cool down to room temperature and recrystallized

from water to yield a dark solid. The product analysed as $[\text{Rh}(\mathbf{1})_2]\text{Cl}_3$ (71.9 mg, 0.0728 mmol, 69.3%). ^1H NMR (500 MHz, D_2O) δ/ppm : 9.31 (s, 4H, $\text{H}^{\text{B}3}$), 8.84 (d, $J = 8.1$ Hz, 4H, $\text{H}^{\text{A}3}$), 8.35 (ddd, 4H, $J = 8.9, 6.8, 1.5$ Hz, $\text{H}^{\text{A}4}$), 8.22–8.15 (m, 4H, $\text{H}^{\text{C}2}$), 8.11–8.05 (m, 4H, $\text{H}^{\text{C}3}$), 7.82 (d, $J = 5.6$ Hz, 4H, $\text{H}^{\text{A}6}$), 7.57 (ddd, $J = 7.3, 5.6, 1.5$ Hz, 4H, $\text{H}^{\text{A}5}$). ^1H NMR (500 MHz, TFA-*d*) δ/ppm : 9.27 (s, 4H, $\text{H}^{\text{B}3}$), 8.90 (d, $J = 8.0$ Hz, 4H, $\text{H}^{\text{A}3}$), 8.34–8.27 (m, 12H, $\text{H}^{\text{A}4+\text{C}2+\text{C}3}$), 7.87 (d, $J = 5.7$ Hz, 4H, $\text{H}^{\text{A}6}$), 7.59 (ddd, $J = 7.5, 5.7, 1.3$ Hz, 4H, $\text{H}^{\text{A}5}$). $^{13}\text{C}\{^1\text{H}\}$ NMR (126 MHz, TFA-*d*) δ/ppm : 156.7 ($\text{C}^{\text{B}4}$), 156.6 ($\text{C}^{\text{A}2}$), 154.3, ($\text{C}^{\text{B}2}$) 152.1 ($\text{C}^{\text{A}6}$), 143.4 ($\text{C}^{\text{A}4}$), 138.6 ($\text{C}^{\text{C}1}$), 132.7 ($\text{C}^{\text{C}3}$), 132.0 ($\text{C}^{\text{C}4}$), 130.8 ($\text{C}^{\text{A}5}$), 128.0 ($\text{C}^{\text{C}2}$), 127.8 ($\text{C}^{\text{A}3}$), 124.8 ($\text{C}^{\text{B}3}$). MALDI: m/z 390.1 $[(\mathbf{1}) + \text{H}]^+$ (calc. 390.1), 492.0 $[\text{Rh}(\mathbf{1})]^+$ (calc. 492.0), 681.0 $[\text{Rh}(\mathbf{1}) + \text{CHCA}]^+$ (calc. 681.0), 881.0 $[\text{Rh}(\mathbf{1})_2]^+$ (calc. 881.1), 903.0 $[\text{Rh}(\mathbf{1})((\mathbf{1})-\text{H})\text{Na}]^+$ (calc. 903.1).

Synthesis of $[\text{Rh}(\mathbf{1})_2]\text{Cl}_3$

$[\text{Rh}(\mathbf{1})_2]\text{Cl}_3$ was prepared in an analogous manner to $[\text{Rh}(4'\text{-Phtpy})_2][\text{PF}_6]_3$.¹⁵ Ligand **1** (300 mg, 0.771 mmol, 2 eq.) was dispersed through sonication for 10 min in ethanol: water (1 : 1, 50 mL). $\text{RhCl}_3 \cdot 3\text{H}_2\text{O}$ (101 mg, 0.384 mmol, 1 eq.) was added. The solution was stirred at reflux (95 °C) for 5 h. The reaction mixture was allowed to cool down to room temperature and a precipitate formed which was filtered off and washed with water (3 × 10 mL), ethanol (3 × 10 mL) and Et_2O (3 × 10 mL). $[\text{Rh}(\mathbf{1})_2]\text{Cl}_3$ (285 mg, 0.288 mmol, 75.0%) was collected as a black solid. ^1H NMR (500 MHz, D_2O) δ/ppm : 9.31 (s, 4H, $\text{H}^{\text{B}3}$), 8.84 (d, $J = 8.1$ Hz, 4H, $\text{H}^{\text{A}3}$), 8.35 (ddd, 4H, $J = 8.1, 5.6, 1.4$ Hz, $\text{H}^{\text{A}4}$), 8.22–8.16 (m, 4H, $\text{H}^{\text{C}2}$), 8.12–8.04 (m, 4H, $\text{H}^{\text{C}3}$), 7.82 (d, $J = 5.6$ Hz, 4H, $\text{H}^{\text{A}6}$), 7.57 (ddd, $J = 7.5, 5.7, 1.4$ Hz, 4H, $\text{H}^{\text{A}5}$). ^1H NMR (500 MHz, TFA-*d*) δ/ppm : 9.31 (s, 4H, $\text{H}^{\text{B}3}$), 8.94 (d, $J = 8.0$ Hz, 4H, $\text{H}^{\text{A}3}$), 8.41–8.29 (m, 12H, $\text{H}^{\text{A}4+\text{C}2+\text{C}3}$), 8.01 (d, $J = 5.5$ Hz, 4H, $\text{H}^{\text{A}6}$), 7.64 (dd, $J = 8.0, 5.6, 1.4$ Hz, 4H, $\text{H}^{\text{A}5}$). $^{13}\text{C}\{^1\text{H}\}$ NMR (126 MHz, TFA-*d*) δ/ppm : 159.1 ($\text{C}^{\text{B}4}$), 158.9 ($\text{C}^{\text{A}2}$), 156.4, ($\text{C}^{\text{B}2}$) 154.5 ($\text{C}^{\text{A}6}$), 145.5 ($\text{C}^{\text{A}4}$), 141.2 ($\text{C}^{\text{C}1}$), 134.9 (d, $J_{\text{PC}} = 11.4$ Hz, $\text{C}^{\text{C}3}$), 133.1 (d, $J_{\text{PC}} = 194$ Hz, $\text{C}^{\text{C}4}$), 132.9 ($\text{C}^{\text{A}5}$), 130.3 (d, $J_{\text{PC}} = 16.4$ Hz, $\text{C}^{\text{C}2}$), 130.0 ($\text{C}^{\text{A}3}$), 127.3 ($\text{C}^{\text{B}3}$). MALDI: m/z 390.2 $[(\mathbf{1}) + \text{H}]^+$ (calc. 390.1), 492.0 $[\text{Rh}(\mathbf{1})]^+$ (calc. 492.0), 527.0 $[\text{Rh}(\mathbf{1}) + \text{Cl}]^+$ (calc. 527.0), 681.1 $[\text{Rh}(\mathbf{1}) + \text{CHCA}]^+$ (calc. 681.0), 881.1 $[\text{Rh}(\mathbf{1})_2]^+$ (calc. 881.1), 903.2 $[\text{Rh}(\mathbf{1})((\mathbf{1})-\text{H}) + \text{Na}]^+$ (calc. 903.1). Found C 48.85, H 3.54, N 7.99; $\text{C}_{42}\text{H}_{38}\text{Cl}_3\text{N}_6\text{O}_9\text{P}_2\text{Rh}$ ($[\text{Rh}(\mathbf{1})_2]\text{Cl}_3 \cdot 3\text{H}_2\text{O}$), requires C 48.41, H 3.68, N 8.07.

Synthesis of $[\text{Rh}(\mathbf{5})_2][\text{PF}_6]_3$

$[\text{Rh}(\mathbf{5})_2]\text{Cl}_3$ was prepared in an analogous manner to $[\text{Rh}(4'\text{-Phtpy})_2][\text{PF}_6]_3$.¹⁵ Compound **5** (150 mg, 0.337 mmol, 2 eq.) was dispersed through sonication for 10 min in ethanol : water (1 : 1, 35 mL). $\text{RhCl}_3 \cdot 3\text{H}_2\text{O}$ (44.2 mg, 0.168 mmol, 1 eq.) was added. The solution was stirred at reflux (95 °C) for 5 h. The reaction mixture was allowed to cool down to room temperature. The solution was filtered and NH_4PF_6 (82.2 mg, 0.504 mmol, 3 eq.) was added to the filtrate under stirring. A precipitate formed which was filtered off and washed with cold water (3 × 1 mL), cold EtOH (3 × 1 mL) and cold Et_2O (3 × 1 mL). $[\text{Rh}(\mathbf{5})_2][\text{PF}_6]_3$ (198 mg, 0.139 mmol, 82.7%) was collected as a pale pink solid. ^1H NMR (500 MHz, CD_3CN) δ/ppm : 9.14 (s, 4H, $\text{H}^{\text{B}3}$), 8.77 (dd, $J = 8.1, 1.4$ Hz, 4H, $\text{H}^{\text{A}3}$), 8.36–8.28 (m, 8H, $\text{H}^{\text{A}4+\text{C}2}$), 8.21–8.15 (m, 4H, $\text{H}^{\text{C}3}$), 7.75 (d, $J = 5.6$ Hz, 4H,

$\text{H}^{\text{A}6}$), 7.53 (ddd, $J = 7.4, 5.6, 1.4$ Hz, 4H, $\text{H}^{\text{A}5}$). $^{13}\text{C}\{^1\text{H}\}$ NMR (126 MHz, CD_3CN) δ/ppm : 157.7 ($\text{C}^{\text{A}2}$), 156.4 ($\text{C}^{\text{B}4}$), 154.9, ($\text{C}^{\text{B}2}$) 153.9 ($\text{C}^{\text{A}6}$), 143.8 ($\text{C}^{\text{A}4}$), 140.0 ($\text{C}^{\text{C}1}$), 133.7 (d, $J_{\text{PC}} = 9.9$ Hz, $\text{C}^{\text{C}3}$), 133.5 (d, $J_{\text{PC}} = 187$ Hz, $\text{C}^{\text{C}1}$), 131.2 ($\text{C}^{\text{A}5}$), 129.6 (d, $J_{\text{PC}} = 14.9$ Hz, $\text{C}^{\text{C}2}$), 128.6 ($\text{C}^{\text{A}3}$), 126.3 ($\text{C}^{\text{B}3}$), 63.4 (C^{A}), 16.7 (C^{B}). $^{31}\text{P}\{^1\text{H}\}$ NMR (200 MHz, CD_3CN) δ/ppm : 16.06 (s, 2P, $\text{P}(\text{O})(\text{OEt})_2$), -144.66 (heptet, $J_{\text{PF}} = 707$ Hz, 3P, $[\text{PF}_6]^-$). MALDI: m/z , 446.1 $[(\mathbf{5}) + \text{H}]^+$ (calc. 446.2), 548.0 $[\text{Rh}(\mathbf{5})]^+$ (calc. 548.1), 737.1 $[\text{Rh}(\mathbf{5}) + \text{CHCA}]^+$ (calc. 737.1) 993.1 $[\text{Rh}(\mathbf{5})_2]^+$ (calc. 993.2), 1283.9 $[\text{Rh}(\mathbf{5})_2 + (\text{PF}_6)_2]^+$ (calc. 1283.2). ESI-MS: negative mode: m/z 145.06 $[\text{PF}_6]^-$ (calc. 144.96); positive mode: 331.26 $[\text{Rh}(\mathbf{5})_2]^{3+}$ (calc. 331.07), 569.27 $[\text{Rh}(\mathbf{5})_2 + (\text{PF}_6)]^{2+}$ (calc. 569.09), 993.15 $[\text{Rh}(\mathbf{5})_2]^+$ (calc. 993.22), 1283.08 $[\text{Rh}(\mathbf{5})_2 + (\text{PF}_6)_2]^+$ (calc. 1283.14). HR ESI-MS: m/z , 331.0721 $[\text{Rh}(\mathbf{5})_2]^{3+}$ (calc. 331.0716), 496.1035 $[\text{Rh}(\mathbf{5})((\mathbf{5})-\text{H})]^{2+}$ (calc. 493.1038), 569.0895 $[\text{Rh}(\mathbf{5})_2 + (\text{PF}_6)]^{2+}$ (calc. 569.0898), 1283.1423 $[\text{Rh}(\mathbf{5})_2 + (\text{PF}_6)_2]^+$ (calc. 1283.1444). UV-VIS (MeCN, 2.25×10^{-5} mol dm^{-3} , λ/nm ($\epsilon/\text{dm}^3 \text{ mol}^{-1} \text{ cm}^{-1}$): 243 (39 600), 284 (sh, 53 500), 295 (60 500), 329 (35 400), 342 (sh, 28 500), 361 (17 400).

Crystallography

Single crystal data were collected on a Bruker APEX-II diffractometer (CuK α radiation) with data reduction, solution and refinement using the programs APEX,¹⁶ ShelXT,¹⁷ Olex2 (ref. 18) and ShelXL v. 2014/7.¹⁹ Structure analysis including the ORTEP representation, used CSD Mercury 2020.1.²⁰ In the structure of $[\text{Rh}(\mathbf{1})_2][\text{NO}_3]_3 \cdot 1.25[\text{H}_3\text{O}][\text{NO}_3] \cdot 2.75\text{H}_2\text{O}$, there are a large number of disordered water molecules, and one $[\text{NO}_3]^-$ position is partially occupied. For charge balance, $1.25\text{H}_2\text{O}$ were treated as $[\text{H}_3\text{O}]^+$; this is reasonable because crystals were grown from concentrated HNO_3 . In $[\text{Rh}(\mathbf{5})_2][\text{PF}_6]_3 \cdot \text{MeCN}$, due to high thermal motion, restraints were applied to two disordered ethoxy groups. Each phenylene ring was disordered and was modelled over two positions, 0.5 : 0.5 and 0.75 : 0.25 site occupancies, respectively. Each MeCN molecule was modelled with an occupancy of 0.5.

Crystal data for $[\text{Rh}(\mathbf{1})_2][\text{NO}_3]_3 \cdot 1.25[\text{H}_3\text{O}][\text{NO}_3] \cdot 2.75\text{H}_2\text{O}$. $\text{C}_{42}\text{H}_{41.25}\text{N}_{10.25}\text{O}_{22.75}\text{P}_2\text{Rh}$, $M_r = 1218.45$, brown block, triclinic, $P\bar{1}$, $a = 12.5277(7)$, $b = 14.3560(8)$, $c = 15.7458(9)$ Å, $\alpha = 91.845(2)^\circ$, $\beta = 110.580(2)^\circ$, $\gamma = 110.494(2)^\circ$, $V = 2444.1(2)$ Å³, $T = 150$ K, $Z = 2$, $\mu(\text{CuK}\alpha) = 4.300$ mm⁻¹. Total 23 158 reflections, 8879 unique ($R_{\text{int}} = 0.0238$). Refinement of 8743 reflections (712 parameters) with $I > 2\sigma(I)$ converged at final $R_1 = 0.0486$ (R_1 all data = 0.0490), $wR_2 = 0.1365$ (wR_2 all data = 0.1371), $\text{gof} = 1.085$. CCDC 2040345.

Crystal data for $[\text{Rh}(\mathbf{5})_2][\text{PF}_6]_3 \cdot \text{MeCN}$. $\text{C}_{52}\text{H}_{51}\text{F}_{18}\text{N}_7\text{O}_6\text{P}_5\text{Rh}$, $M_r = 1469.76$, colourless plate, triclinic, $P\bar{1}$, $a = 12.2477(7)$, $b = 14.0636(8)$, $c = 19.8182(11)$ Å, $\alpha = 73.903(4)^\circ$, $\beta = 83.442(4)^\circ$, $\gamma = 82.315(3)^\circ$, $V = 3239.6(3)$ Å³, $T = 150$ K, $Z = 2$, $\mu(\text{CuK}\alpha) = 4.223$ mm⁻¹. Total 37 630 reflections, 11 469 unique ($R_{\text{int}} = 0.0431$). Refinement of 9490 reflections (845 parameters) with $I > 2\sigma(I)$ converged at final $R_1 = 0.1061$ (R_1 all data = 0.1189), $wR_2 = 0.2968$ (wR_2 all data = 0.3092), $\text{gof} = 1.071$. CCDC 2025772.

Synthesis of $\text{Rh}(\mathbf{1})_2@ \text{TiO}_2$ NPs

Method 1. $(\mathbf{1})@ \text{TiO}_2$ NPs (440 mg, 0.05 mmol, 2 eq.) were dispersed through sonication for 10 min in ethanol: water (1 : 1,

5 mL). $\text{RhCl}_3 \cdot 3\text{H}_2\text{O}$ (6.58 mg, 0.0250 mmol, 1 eq.) was added. The suspension was stirred at reflux (95 °C) for 5 h. The reaction mixture was allowed to cool down to room temperature. The $\text{Rh}(\mathbf{1})_2@/\text{TiO}_2$ NPs were separated from the solvent by centrifugation (10 min, 9000 rpm) and then washed with water (2 × 8 mL) and ethanol (2 × 8 mL) and then dried under high vacuum yielding a light red powder (428 mg). $\text{Rh}(\mathbf{1})_2@/\text{TiO}_2$ NPs (5–10 mg) was dispersed in 500 μL D_2O in an NMR tube. MALDI spectrum of dried $\text{Rh}(\mathbf{1})_2@/\text{TiO}_2$ NPs: m/z 390.1 $[(\mathbf{1}) + \text{H}]^+$ (calc. 390.1), 492.0 $[\text{Rh}(\mathbf{1})]^+$ (calc. 492.0), 527.0 $[\text{Rh}(\mathbf{1}) + \text{Cl}]^+$ (calc. 527.0), 681.1 $[\text{Rh}(\mathbf{1}) + \text{CHCA}]^+$ (calc. 681.0), 881.1 $[\text{Rh}(\mathbf{1})_2]^+$ (calc. 881.1). Solid-state UV-VIS (λ/nm): 411, 608, 669.

Method 2. $(\mathbf{1})@/\text{TiO}_2$ NPs (440 mg, 0.05 mmol, 2 eq.) were dispersed with NaCl (14.6 mg, 0.25 mmol, 10 eq.) through sonication for 10 min in ethanol (5 mL). $[\text{Rh}_2(\mu\text{-OAc})_4(\text{H}_2\text{O})_2]$ (12 mg, 0.0251 mmol, 1 eq.) was added. Argon was bubbled through the suspension for 5 min while stirring. The suspension was stirred under argon at 80 °C for 18 h. The reaction mixture was allowed to cool down to room temperature. The $\text{Rh}(\mathbf{1})_2@/\text{TiO}_2$ NPs were separated from the solvent by centrifugation (10 min, 9000 rpm) and then washed with water (2 × 8 mL) and ethanol (2 × 8 mL). The $\text{Rh}(\mathbf{1})_2@/\text{TiO}_2$ NPs were dried under high vacuum yielding a light brown powder (430 mg). $\text{Rh}(\mathbf{1})_2@/\text{TiO}_2$ NPs (5–10 mg) was dispersed in 500 μL D_2O in an NMR tube. MALDI spectrum of dried $\text{Rh}(\mathbf{1})_2@/\text{TiO}_2$ NPs: m/z 390.1 $[(\mathbf{1}) + \text{H}]^+$ (calc. 390.1), 492.1 $[\text{Rh}(\mathbf{1})]^+$ (calc. 492.0), 527.1 $[\text{Rh}(\mathbf{1}) + \text{Cl}]^+$ (calc. 527.0), 681.1 $[\text{Rh}(\mathbf{1}) + \text{CHCA}]^+$ (calc. 681.0). Solid-state UV-VIS (λ/nm): 444, 539, 609, 664.

Oxidation of *rac*-(1R)-1-phenylethanol to acetophenone in water under air

$\text{Rh}(\mathbf{1})_2@/\text{TiO}_2$ NPs (72.7 mg, 0.5 mol%) and milliQ water (1.67 mL) were added to a microwave vial. The contents were sonicated (1 min) and then aqueous NaOH (25 mM, 0.331 mL) and *rac*-(1R)-1-phenylethanol (0.1 mL, 0.827 mmol, 1 eq.) were added to the suspension. The vial was sealed and the reaction mixture was heated to 100 °C for 24 h. A small amount of the reaction mixture (*ca.* 50 μL) was removed by syringe and dispersed in 500 μL D_2O in an NMR tube. ^1H NMR spectra were measured to determine product : reactant ratios. The NMR spectroscopic data revealed that after 18 h, the ratio of product to reactant was 1.0 : 5.7 (14.9% product). The sampling procedure was repeated with 24 h and 38 h reaction time yielding a ratio of 1 : 3.3 (23.2% product, Table S1†) and 1 : 2.9 (25.7% product) respectively. The procedure yielded similar conversions independent of the synthetic route of the catalytic NPs.

Recyclability of $\text{Rh}(\mathbf{1})_2@/\text{TiO}_2$ NPs

$\text{Rh}(\mathbf{1})_2@/\text{TiO}_2$ NPs (72.7 mg, 0.5 mol%) and milliQ water (1.67 mL) were added to a microwave vial. The suspension was sonicated (1 min) and then aqueous NaOH (25 mM, 0.331 mL) was added. The pH of the mixture was determined to be 7.8. *rac*-(1R)-1-Phenylethanol (0.1 mL, 0.827 mmol, 1 eq.) was added to the suspension after which the vial was sealed and the reaction

mixture heated to 100 °C for 24 h. After cooling, the reaction mixture was washed with Et_2O (6 × 3 mL). A small amount of the collected Et_2O fractions (*ca.* 50 μL) was removed by syringe and the solvent was evaporated. The residue was dissolved in 500 μL D_2O and added to an NMR tube. The ^1H NMR spectrum was measured to determine product : reactant ratios. The pH of the reaction mixture was measured using a pH electrode and adjusted to the initial value of 7.8 by adding aqueous NaOH (25 mM). The vial was resealed and the reaction mixture was heated again to 100 °C for 24 h. The reaction was performed with this procedure 5 times in total. The product conversions were as follows: 20.3, 20.1, 18.3, 20.9 and 19.9%.

Kinetics of oxidation

$\text{Rh}(\mathbf{1})_2@/\text{TiO}_2$ NPs (145.4 mg, 0.5 mol%) and D_2O (3.33 mL) were added into a microwave vial. The contents were sonicated (1 min) and then NaOH (25 mM in D_2O , 0.667 mL) and *rac*-(1R)-1-phenylethanol (0.2 mL, 1.65 mmol, 1 eq.) were added to the suspension. The vial was sealed and the reaction mixture was heated to 100 °C for two weeks (*ca.* 300 h). At varying time intervals, a small amount of the reaction mixture (*ca.* 50 μL) was removed by syringe and dispersed in 500 μL D_2O in an NMR tube. The ^1H NMR spectrum was recorded to determine the product : reactant ratios at any point. Overall, data for 27 points were recorded over 12 days.

Control experiment 1: catalyst influence on reaction rate

Activated NPs (72.7 mg) and milliQ water (1.67 mL) were added to a microwave vial. The contents were sonicated (1 min) and then aqueous NaOH (25 mM, 0.331 mL) and *rac*-(1R)-1-phenylethanol (0.1 mL, 0.827 mmol, 1 eq.) were added to the suspension. The vial was sealed and the reaction mixture was heated to 100 °C for 24 h. A small amount of the reaction mixture (*ca.* 50 μL) was removed by syringe and dispersed in 500 μL D_2O in an NMR tube. The ^1H NMR spectrum was recorded and revealed that no acetophenone had formed. Further control experiments were conducted using either unactivated commercial NPs, activated NPs, $(\mathbf{1})@/\text{TiO}_2$ NPs or $[\text{Rh}_2(\mu\text{-OAc})_4(\text{H}_2\text{O})_2]$. The control experiment using $(\mathbf{1})@/\text{TiO}_2$ NPs and $[\text{Rh}_2(\mu\text{-OAc})_4(\text{H}_2\text{O})_2]$ showed 7% product conversion while all other experiments showed less than 1% product conversion after 24 hours (Table S1†).

Control experiment 2: temperature influence on reaction rate

$\text{Rh}(\mathbf{1})_2@/\text{TiO}_2$ NPs (72.7 mg, 0.5 mol%) and milliQ water (1.67 mL) were added to a microwave vial. The contents were sonicated (1 min) and then aqueous NaOH (25 mM, 0.331 mL) and *rac*-(1R)-1-phenylethanol (0.1 mL, 0.827 mmol, 1 eq.) were added to the suspension. The vial was sealed and the reaction mixture was left stirring at room temperature for 72 h. A small amount of the reaction mixture (*ca.* 50 μL) was removed by syringe and dispersed in 500 μL D_2O in an NMR tube. The ^1H NMR spectrum was recorded which revealed no acetophenone had formed (Table S1†).

Control experiment 3: NaOH influence on functionalization stability

Rh(1)₂@TiO₂ NPs (72.7 mg, 0.5 mol%) and milliQ water (1.67 mL) were added to a microwave vial. The contents were sonicated (1 min) and then aqueous NaOH (25 mM, 0.331 mL) was added to the suspension. The vial was sealed and the reaction mixture was heated to 100 °C for 72 h. The supernatant solution was separated from the NPs by centrifugation (30 min, 17 500 rpm). The supernatant solution was filtered and added into a separate microwave vial and *rac*-(1*R*)-1-phenylethanol (0.1 mL, 0.827 mmol, 1 eq.) was added to the solution. The vial was sealed and the reaction mixture was heated to 100 °C for 24 hours. A small amount of the reaction mixture (*ca.* 500 μL) was removed by syringe and dispersed in 500 μL D₂O in an NMR tube. The ¹H NMR spectrum was recorded and revealed that no acetophenone had formed. The separated NPs were added together with milliQ water (1.67 mL) into a separate microwave vial. The contents were sonicated (1 min) and then aqueous NaOH (25 mM, 0.331 mL) *rac*-(1*R*)-1-phenylethanol (0.1 mL, 0.827 mmol, 1 eq.) were added to the suspension. The vial was sealed and the reaction mixture was heated to 100 °C for 24 hours. A small amount of the reaction mixture (*ca.* 50 μL) was removed by syringe and dispersed in 500 μL D₂O in an NMR tube. The ¹H NMR spectrum was recorded and showed acetophenone had been formed. This experiment was repeated without any base and yielded the same result. The reaction using the separated supernatant solution did not show acetophenone formation (<1%) while the reaction containing the separated NPs showed normal product conversion (19.9%).

Control experiment 4: NaOH concentration influence on reaction rate

Rh(1)₂@TiO₂ NPs (72.7 mg, 0.5 mol%) and milliQ water (1.67 mL) were added to a microwave vial. The contents were sonicated (1 min) and then aqueous NaOH (25 mM, 0.331 mL) *rac*-(1*R*)-1-phenylethanol (0.1 mL, 0.827 mmol, 1 eq.) were added to the suspension. Simultaneously three other vials were prepared under the same conditions with different NaOH (0.331 mL, 50 mM, 0.25 M, 2.5 M) concentrations. The vials were sealed and the reaction mixtures were heated to 100 °C for 3 weeks. A small amount of each reaction mixture (*ca.* 50 μL) was removed from each vial by syringe and dispersed in 500 μL D₂O in separate NMR tubes. The ¹H NMR spectrum of each sample was recorded to determine the product : reactant ratios at any point. Overall, 11 data points were recorded over 24 days.

Control experiment 5: oxidation using free rhodium complexes

[Rh(1)₂]Cl₃ (3.79 mg, *ca.* 0.5 mol%) and milliQ water (1.67 mL) were added to a microwave vial. The contents were sonicated (1 min) and then aqueous NaOH (25 mM, 0.331 mL) and *rac*-(1*R*)-1-phenylethanol (0.1 mL, 0.827 mmol, 1 eq.) were added to the suspension. The vial was sealed and the reaction mixture was left stirring at 100 °C for 24 h. A small amount of the reaction mixture (*ca.* 50 μL) was removed by syringe and dispersed in 500

μL D₂O in an NMR tube. The NMR data revealed that after 24 h, the ratio of product to reactant was 1.0 : 5.3 (15.8% product, Table S1†). The procedure was repeated using [Rh(5)₂][PF₆]₃ and showed a ratio of product to reactant of 1.0 : 4.2 (19.2% product, Table S1†).

Control experiment 6: inert atmosphere and light influence on reaction rate

Four microwave vials were prepared to all of them Rh(1)₂@TiO₂ NPs (72.7 mg, 0.5 mol%) and milliQ water (1.67 mL) was added. The contents were sonicated (1 min) and then aqueous NaOH (25 mM, 0.331 mL) and *rac*-(1*R*)-1-phenylethanol (0.1 mL, 0.827 mmol, 1 eq.) were added to the suspensions. The suspensions in two vials were bubbled with Argon for 15 minutes. The vials were sealed and one under inert atmosphere and one under air were covered from light with alumina foil. Leading to vials having inert atmosphere, no light, inert atmosphere and no light, and a control with air not covered from light. The four vials were left stirring at 100 °C for 72 h. A small amount of each reaction mixture (*ca.* 50 μL) was removed by syringe and dispersed in 500 μL D₂O in separate NMR tubes. The NMR data revealed that after 72 h, the ratio of product to reactant for the control vial was 1.0 : 2.4 (29.3% product, Table S1†) while the ratio of product to reactant when using inert gas was 1.0 : 5.0 (16.5% product, Table S1†). Performing the reaction without light had no effects on the product formation.

Results and discussion

Choice of anchoring ligand and substrate

2,2':6',2''-Terpyridines (tpy) are well-established chelating ligands which undergo a conformational change from the equilibrium transoid-arrangement upon coordination to metal centres.²¹ The tpy metal-binding domain acts as a good σ-donor and a strong π-acceptor, making tpy ligands excellent candidates for the stabilization of low oxidation state metal centres. This leads to their applications in a wide range of homogeneous catalytic reactions involving metals such as Ni, Cu, Ru, Pd, Rh, Fe, Mg and Co.²²

The functionalization of metal chalcogenide NPs with carboxylic and phosphonic acids is well-established.^{23–32} We have extended surface-modification strategies developed for dye-sensitized solar cells to nanoparticles and have illustrated that TiO₂ NPs can be functionalized with bpy or tpy ligands bearing carboxylic or phosphonic acid anchoring units.¹¹ We further demonstrated the preferential binding of phosphonic acids over carboxylic acids, and the ability of ligand-functionalized NPs to complex metal ions such as copper(II) and iron(II) to form robust coordination-complex functionalized NPs.¹¹

TiO₂ NPs have benefits beyond being able to strongly bind anchoring ligands (carboxylic or phosphonic acids): they comprise earth abundant elements, are relatively cheap, non-toxic, thermodynamically stable and temperature resistant. TiO₂ NPs can also be specifically prepared in a wide variety of

sizes and shapes. This makes them a desirable choice for further investigation as a substrate for catalysis.

One potential problem with TiO₂ NPs is that they can exhibit large amounts of surface-adsorbed water creating problems for catalytic processes in which it is crucial to avoid exposure to water and redox-related species such as dioxygen.^{11,22} It is therefore of significant interest to investigate catalytic systems that can tolerate both water and air.¹² These “green” conditions are in any case desirable. The rhodium(III) complexes selected for the present investigation are tolerant of both water and air.

Attempted synthesis of [Rh₂Cl₂(μ-OAc)(1)₂]Cl and synthesis of [Rh(1)₂]Cl₃

Wang and coworkers have reported the catalytic behaviour of the water-soluble complex [Rh₂Cl₂(μ-OAc)(tpy)₂]Cl in the dehydrogenation and oxidation of alcohols in aqueous aerobic conditions to carboxylic acids or ketones.¹² Our initial aim, was to prepare a TiO₂ NP surface-bound version of this catalyst containing [Rh₂Cl₂(μ-OAc)(1)₂]⁺. Before investigating the metallation of (1)@TiO₂ NP, we decided to prepare [Rh₂(μ-OAc)(1)₂Cl₂]Cl following the general procedure of Wang and coworkers, starting from [Rh₂(μ-OAc)₄(H₂O)₂] and **1** in the presence of NaCl in EtOH. A black product was isolated and the MALDI mass spectrum (Fig. S1[†]) showed peaks at *m/z* 492.0, 681.0, 881.1 and 903.0 corresponding to [Rh(1)]⁺, [Rh(1) + CHCA]⁺, [Rh(1)₂]⁺ and [Rh(1)((1)-H) + Na]⁺. No peaks assigned to acetato species were observed in the mass spectrum and the ¹H NMR spectrum (Fig. S2[†]) showed no signals arising from an acetate group.

A comparison of the ¹H NMR spectrum of **1** with that of the black product suggested the formation of a homoleptic [Rh(1)₂]³⁺ complex. The shift to lower frequency for the signal assigned to proton A6 (see Scheme 1) is consistent with this proton lying over the ring of a second tpy domain and the spectrum (which shows only one set of tpy signals) indicates the formation of a homoleptic bis(tpy) complex. We therefore concluded that the product was [Rh(1)₂]Cl₃. In order to confirm this proposal, we adapted the protocol described by Thomas and coworkers¹⁵ for the preparation of [Rh(4'-Phtpy)₂][PF₆]₃ to prepare [Rh(1)₂]Cl₃ from RhCl₃·3H₂O and **1**. The presence of chloride counter ion in the product was established by dissolving the compound in concentrated HNO₃ and adding a drop of silver nitrate which lead to the precipitation of white silver chloride (Fig. S3[†]). The MALDI mass spectrum of [Rh(1)₂]Cl₃ (Fig. S4[†]) was similar to that described above (Fig. S2[†]) with peaks at *m/z* 492.0, 527.0, 681.1, 881.1 and 903.2 arising from [Rh(1)]⁺, [Rh(1)Cl]⁺, [Rh(1) + CHCA]⁺, [Rh(1)₂]⁺ and [Rh(1)((1)-H) + Na]⁺. The ¹H and ¹³C NMR spectra of [Rh(1)₂]Cl₃ (Fig. S5 and S6[†]) were assigned using 2D methods (Fig. S7–S9[†]) and were identical to those of the product from the attempted synthesis of [Rh₂(μ-OAc)(1)₂Cl₂]Cl (Fig. S10–S13[†]). We speculate that the acidic phosphonic acid substituents on ligand **1** labilize the acetato ligands and prevent the isolation of [Rh₂Cl₂(μ-OAc)(1)₂]⁺.

The compound [Rh(1)₂]Cl₃ formed during the synthesis was insoluble in most solvents and could only be dissolved in

concentrated HNO₃ or in water under very basic conditions. This pH dependent solubility suggested the formation of a zwitterionic species in basic conditions.

Crystal structure of [Rh(1)₂][NO₃]₃·1.25[H₃O][NO₃]₃·2.75H₂O

Single crystals of [Rh(1)₂][NO₃]₃·1.25[H₃O][NO₃]₃·2.75H₂O grew from a solution of [Rh(1)₂]Cl₃ dissolved in a small amount of concentrated aqueous HNO₃ which, after the addition of water, was left to stand at room temperature (*ca.* 22 °C) for 4 weeks. The complex crystallizes in the triclinic space group *P* $\bar{1}$ and the single crystal structure confirmed the fully protonated phosphonic acid substituents. The crystal lattice contained a large number of disordered H₂O molecules, as well as [H₃O]⁺ and [NO₃]⁻ in addition to the nitrate ions required to balance the charge on the [Rh(1)₂]³⁺ cation. Because of the disorder, we focus only on the structure of the cation (Fig. 1a). An ORTEP

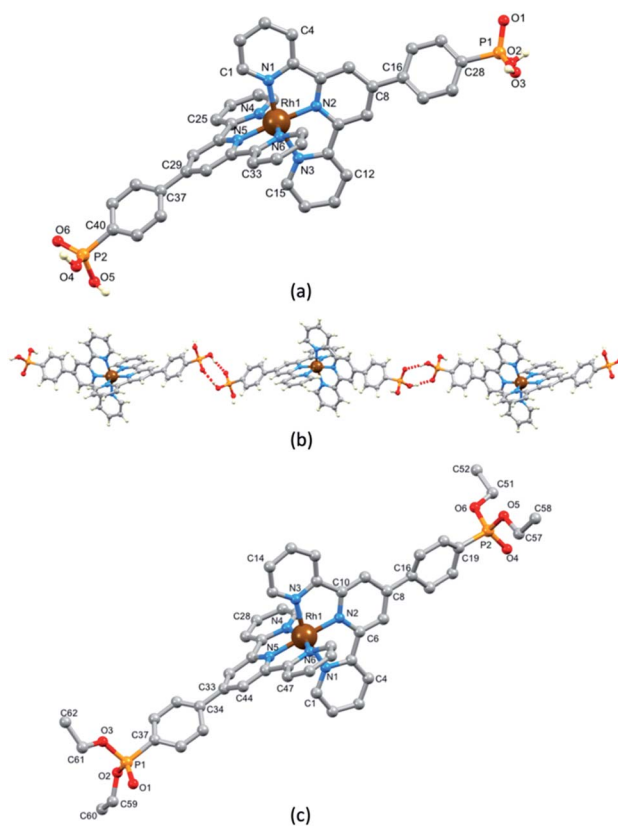


Fig. 1 (a) The structure of the [Rh(1)₂]³⁺ cation in the complex [Rh(1)₂][NO₃]₃·1.25[H₃O][NO₃]₃·2.75H₂O; H atoms except those in the phosphonic acid groups are omitted for clarity. Selected bond distances: Rh1–N1 = 2.047(3), Rh1–N2 = 1.962(3), Rh1–N3 = 2.055(3), Rh1–N4 = 2.055(3), Rh1–N5 = 1.964(3), Rh1–N6 = 2.043(3), P1–O1 = 1.501(3), P1–O2 = 1.544(3), P1–O3 = 1.552(3), P1–C28 = 1.786(4), P2–O4 = 1.550(3), P2–O5 = 1.546(4), P2–O6 = 1.489(3), P2–C40 = 1.800(4) Å. (b) Part of one hydrogen-bonded chain of [Rh(1)₂]³⁺ cations. (c) The structure of the [Rh(5)₂]³⁺ cation in [Rh(5)₂][PF₆]₃·MeCN; H atoms are omitted for clarity. Selected bond parameters: Rh1–N1 = 2.040(6), Rh1–N2 = 1.964(6), Rh1–N3 = 2.046(7), Rh1–N4 = 2.047(7), Rh1–N5 = 1.984(6), Rh1–N6 = 2.050(7), P1–O1 = 1.471(10), P1–O2 = 1.540(15), P1–O3 = 1.605(14), P1–C37 = 1.803(11), P2–O4 = 1.453(8), P2–O5 = 1.707(15), P2–O6 = 1.634(13), P2–C19 = 1.787(9) Å.

representation of the cation is displayed in Fig. S21a.† The octahedral coordination environment with two chelating tpy domains is unexceptional with the $[\text{Rh}(\text{tpy})_2]$ core closely resembling that observed in other $[\text{Rh}(\text{Xtpy})_2]^{3+}$ cations ($X = 4'$ -phenyl, $4'$ -(pyridin-4-yl), 4-ferrocenyl (DAHDA,¹⁵ DAHDIA,¹⁵ DAHDEW,¹⁵ XIFTIS³⁴). The Rh–N bond lengths are given in the caption to Fig. 1a, and the chelate N–Rh–N bond angles are in the range $79.84(13)$ – $80.60(13)^\circ$. Each P atom is tetrahedrally sited and P–O and P–C bond lengths are given in the caption to Fig. 1a; the bond angles centred on P1 and P2 lie in the range $104.20(17)$ – $114.96(18)^\circ$. The most dominant packing interaction involving the $[\text{Rh}(\mathbf{1})_2]^{3+}$ cations is hydrogen bonding between $\text{PO}(\text{OH})_2$ units leading to the assembly of 1D-chains (Fig. 1b). For the centrosymmetric hydrogen-bonded motifs, pertinent parameters are $\text{O1}\cdots\text{O2}^{\text{i}} = 2.485(5)$ Å, $\text{O1}\cdots\text{H}-\text{O2}^{\text{i}} = 1.68$ Å, angle $\text{O1}\cdots\text{H}-\text{O2}^{\text{i}} = 159^\circ$ (symmetry code $i = -1 - x, -1 - y, 2 - z$), $\text{O4}\cdots\text{O6}^{\text{ii}} = 2.534(5)$ Å, $\text{O4}\cdots\text{HA}-\text{O6}^{\text{ii}} = 1.70$ Å, angle $\text{O4}\cdots\text{HA}-\text{O6}^{\text{ii}} = 171^\circ$ (symmetry code $ii = 1 - x, 2 - y, 1 - z$). Although the $[\text{Rh}(\mathbf{1})_2]^{3+}$ cations pack in the lattice with head-to-tail pairings of ligands on adjacent complexes, there are no significant π -stacking interactions between phenyl and tpy domains.

Synthesis and characterization of $[\text{Rh}(\mathbf{5})_2][\text{PF}_6]_3$

Because of initial uncertainties regarding the protonation state of the homoleptic complex obtained with **1**, we prepared an analogous compound with a phosphonate ester. Compound **5** (Scheme 1) was prepared according to the literature⁴⁵ and its reaction with $\text{RhCl}_3 \cdot 3\text{H}_2\text{O}$ followed by anion exchange using NH_4PF_6 yielded $[\text{Rh}(\mathbf{5})_2][\text{PF}_6]_3$ as a pale pink solid in 82.7% yield. Mass spectrometric and ^1H , ^{13}C and ^{31}P NMR spectroscopic data (see the Experimental section, Fig. S14–S16†) were consistent with the formation of the homoleptic complex. ^1H and ^{13}C NMR spectra were assigned using NOESY, HMQC and HMBC spectra (Fig. S17–S19†). The solution absorption spectrum (in MeCN) of $[\text{Rh}(\mathbf{5})_2][\text{PF}_6]_3$ (Fig. S20†) exhibits intense bands below 370 nm which are assigned to ligand-centred $\pi^* \leftarrow \pi$ transitions similar to that reported for $[\text{Rh}(\text{tpy})_2](\text{PF}_6)_3$.³³ The lack of absorptions in the visible region arising from metal-to-ligand charge transfer is consistent with the low-spin d^6 configuration of the Rh(III) centre. X-ray quality crystals of $[\text{Rh}(\mathbf{5})_2][\text{PF}_6]_3 \cdot \text{MeCN}$ were grown by vapour diffusion of Et_2O into a MeCN solution and the structure of the $[\text{Rh}(\mathbf{5})_2]^{3+}$ cation is shown in Fig. 1c; an ORTEP representation is displayed in Fig. S21b.† Important bond lengths and angles are given in the caption to Fig. 1c. As anticipated, the Rh(III) centre is octahedral, bound by two bis-chelating tpy domains. The structure is unexceptional but serves to confirm the formation of the homoleptic complex, and there are no noteworthy packing interactions.

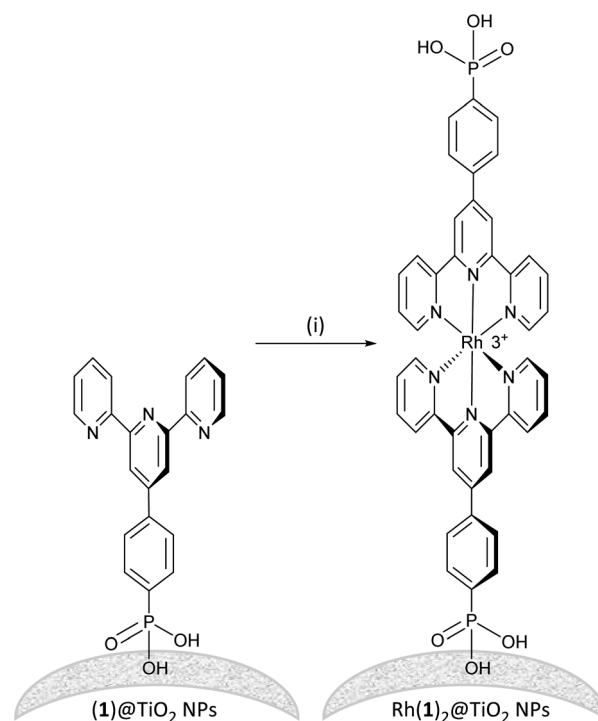
Assembly of a homoleptic rhodium(III) complex on TiO_2 NPs

Established procedures for TiO_2 NP activation involve HNO_3 (ref. 35) treatment and sonication to optimize surface functionalization and particle dispersion respectively.³⁶ Commercial P25 TiO_2 NPs were activated using aqueous HNO_3 and then functionalized with ligand **1** (see the Experimental section). For

the functionalization, an aqueous suspension of dispersed ligand **1** and activated NPs was heated to 130°C for 3 h under microwave conditions. The $(\mathbf{1})@\text{TiO}_2$ NPs were separated from the liquid phase by centrifugation. The functionalization procedure differs only from that previously described¹¹ in that it was scaled up and the ratio TiO_2 to **1** had to be increased by 10% to ensure binding of all the ligand.

To form the NP-supported complex $\text{Rh}(\mathbf{1})_2@\text{TiO}_2$ (Scheme 2), $(\mathbf{1})@\text{TiO}_2$ NPs were dispersed with $\text{RhCl}_3 \cdot 3\text{H}_2\text{O}$ in ethanol and water under air at 95°C for 5 h. The NPs changed colour from white to pale red. The $\text{Rh}(\mathbf{1})_2@\text{TiO}_2$ NPs were separated from the solvent using centrifugation (see Experimental section, Method 1). The conjugate $\text{Rh}(\mathbf{1})_2@\text{TiO}_2$ was also prepared using $[\text{Rh}_2(\mu\text{-OAc})_4(\text{H}_2\text{O})_2]$ as a precursor (see Experimental, Method 2). $(\mathbf{1})@\text{TiO}_2$ NPs were dispersed with NaCl and $[\text{Rh}_2(\mu\text{-OAc})_4(\text{H}_2\text{O})_2]$ in EtOH at 80°C , and a colour change from pale blue to brown was observed during the reaction. The $\text{Rh}(\mathbf{1})_2@\text{TiO}_2$ NPs were separated using centrifugation. The overall charge associated with each $\{\text{Rh}(\mathbf{1})_2\}$ moiety in the $\text{Rh}(\mathbf{1})_2@\text{TiO}_2$ is uncertain as the protonation state and binding mode is typically not well defined.^{37–39} However, assuming that all **1** ligands are fully protonated, the $\text{Rh}(\mathbf{1})_2@\text{TiO}_2$ NPs should bear a +3 charge per surface-bound $\{\text{Rh}(\mathbf{1})_2\}$.

The $\text{Rh}(\mathbf{1})_2@\text{TiO}_2$ NPs from both methods 1 and 2 were characterized using MALDI mass spectrometry and FTIR, ^1H NMR and solid-state UV-VIS spectroscopies. FTIR spectra



Scheme 2 Assembly of $[\text{Rh}(\mathbf{1})_2]^{3+}$ on TiO_2 NPs starting from NPs functionalized with **1**. Conditions: (i) RhCl_3 , EtOH : H_2O , 95°C , 6 h or $[\text{Rh}_2(\mu\text{-OAc})_4(\text{H}_2\text{O})_2]$, NaCl, EtOH, 80°C , 18 h. NP surfaces are rough and could potentially provide two binding sites for the rhodium metal complex or two NPs could come together to form the rhodium metal complex.

(Fig. S22[†]), solid-state absorption spectra (Fig. S23[†]), TGA measurements (Fig. S24 and S25[†]), MALDI mass spectra (Fig. S26 and S27[†]) and ¹H NMR spectra (Fig. S28[†]) confirmed that both methods yielded similar Rh(1)₂@TiO₂ NPs. The characterization details are discussed further below.

Characterization of Rh(1)₂@TiO₂ NPs

The MALDI mass spectrum of Rh(1)₂@TiO₂ NPs⁺ (Fig. S26 and S27[†]) showed peaks at *m/z* 492.1, 527.0 and 681.1 arising from [Rh(1)]⁺, [Rh(1) + Cl]⁺ and [Rh(1) + CHCA]⁺, respectively. Additionally, a peak at *m/z* 881.1 assigned to [Rh(1)₂]³⁺ was observed for Rh(1)₂@TiO₂ NPs prepared using method 1. The similarity between the mass spectrum of pristine [Rh(1)₂]Cl₃ and the mass spectra of Rh(1)₂@TiO₂ NPs is consistent with the assembly of the homoleptic [Rh(1)₂]³⁺ complex on the NP surface using both [Rh₂(μ-OAc)₄(H₂O)₂] and RhCl₃·3H₂O as metal source.

Fig. 2 compares the FT-IR spectra of activated NPs, (1)@TiO₂ NPs and Rh(1)₂@TiO₂ NPs together with the spectrum of the pristine compound [Rh(1)₂]Cl₃. The full spectra are presented in Fig. S29[†]. The activated NPs show weak absorption bands at 1613 and 1584 cm⁻¹ while the (1)@TiO₂ NPs exhibit bands at 1602, 1588, 1570, 1538, 1470, 1444, 1408 and 1387 cm⁻¹. The isolated complex [Rh(1)₂]Cl₃ has absorption bands at 1605, 1565, 1549, 1477, 1429, 1395, 1367, 1297, 1242, 1213, 1152, 1127, 1072, 1048, 1029 and 1015 cm⁻¹. Rh(1)₂@TiO₂ NPs shows bands at 1607, 1585, 1572, 1554, 1476, 1428, 1408, 1391 and 1136 cm⁻¹ and their relative intensities and energies resemble most of the major peaks seen in (1)@TiO₂ NPs and [Rh(1)₂]Cl₃.

Thus, the IR spectroscopic data provide evidence that (1)@TiO₂ NPs has undergone a change upon treatment with either [Rh₂(μ-OAc)₄(H₂O)₂] or RhCl₃·3H₂O consistent with the formation of Rh(1)₂@TiO₂ NPs.

Further evidence for the NP functionalization came from ¹H NMR spectroscopic data for Rh(1)₂@TiO₂ NPs dispersed in D₂O. TiO₂ NPs and their functionalized derivatives are insoluble in D₂O, and signals associated with the surface-bound species are not observed under typical acquisition conditions. Any observed resonances can be attributed to the released compounds

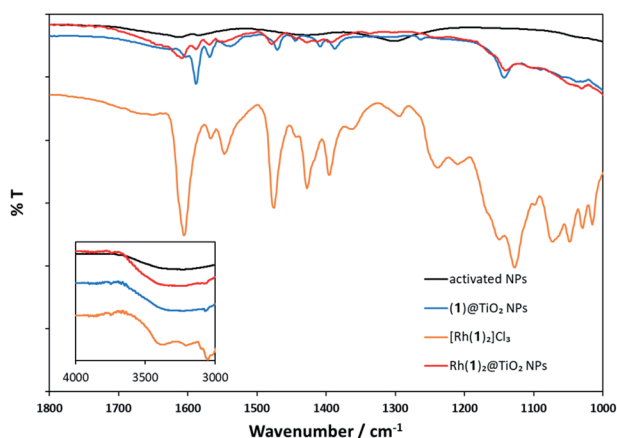


Fig. 2 Solid-state FT-IR spectra of activated NPs (black), (1)@TiO₂ NPs (blue), [Rh(1)₂]Cl₃ (orange), and Rh(1)₂@TiO₂ NPs (red).

from the surface. The ¹H NMR spectrum of Rh(1)₂@TiO₂ NPs synthesized from [Rh₂(μ-OAc)₄(H₂O)₂] (Fig. 3d) showed no signals in the aromatic region. The only signals recorded arose from residual HOD and EtOH (Fig. S28[†]). A similar result was obtained for Rh(1)₂@TiO₂ NPs synthesized with RhCl₃·3H₂O (Fig. 3g). Under very basic conditions with an excess of NaOH, it is possible to partially defunctionalize the surface leading to the appearance of signals arising from free complex and ligand. This can be seen with the Rh(1)₂@TiO₂ NPs synthesized from [Rh₂(μ-OAc)₄(H₂O)₂] (Fig. 3e) or RhCl₃·3H₂O (Fig. 3h). The ¹H NMR spectra of 1 (Fig. 3a), (1)@TiO₂ and [Rh(1)₂]Cl₃ made with [Rh₂(μ-OAc)₄(H₂O)₂] (Fig. 3c) or RhCl₃·3H₂O (Fig. 3f) were also recorded under basic conditions. Using these spectra for comparison, we observed that the spectra of Rh(1)₂@TiO₂ NPs (Fig. 3e and h) contained signals arising from both 1 and [Rh(1)₂]Cl₃. This is not surprising considering that not every surface-bound ligand will bind a metal ion. However the similarity between the spectra of the pristine [Rh(1)₂]Cl₃ (Fig. 3c and f) and those of the defunctionalized NPs (Fig. 3e and h) provides strong evidence that the surface was partially functionalized with [Rh(1)₂]³⁺ prior to treatment with base.

Thermogravimetric analysis (TGA) of activated NPs, (1)@TiO₂ and Rh(1)₂@TiO₂ NPs was carried out, and the results are presented in Fig. 4. All samples show a weight loss of 1.5–2% in two steps (isotherm maxima <120 °C and <330 °C). The two steps can be attributed to the loss of physisorbed followed by chemisorbed water. The mass of the non-functionalized NPs undergoes no further significant change (Fig. S30[†]) upon being heated to 900 °C for 30 minutes. The (1)@TiO₂ NPs and Rh(1)₂@TiO₂ NPs exhibit additional 3% and 4–5% weight losses above ca. 400 °C (Fig. S24 and S25[†]) ascribed to decomposition of the ligand. Additionally, Rh(1)₂@TiO₂ NPs show a weight increase occurring during the 30 minute 900 °C isotherm.

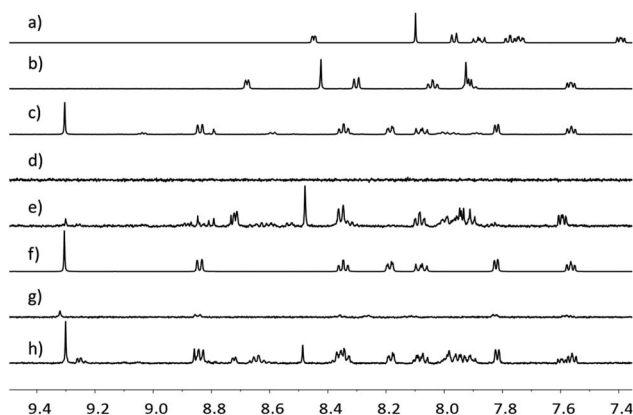


Fig. 3 ¹H NMR spectra (500 MHz, D₂O, 298 K) of 1 in D₂O and NaOH (a), (1)@TiO₂ in D₂O and NaOH (b), [Rh(1)₂]Cl₃ made using [Rh₂(μ-OAc)₄(H₂O)₂] in D₂O and NaOH (c), Rh(1)₂@TiO₂ NPs made using [Rh₂(μ-OAc)₄(H₂O)₂] in D₂O (d), Rh(1)₂@TiO₂ NPs made using [Rh₂(μ-OAc)₄(H₂O)₂] in D₂O and NaOH (e), [Rh(1)₂]Cl₃ made using RhCl₃·3H₂O in D₂O and NaOH (f), Rh(1)₂@TiO₂ NPs made using RhCl₃·3H₂O in D₂O and NaOH (g), Rh(1)₂@TiO₂ NPs made using RhCl₃·3H₂O in D₂O and NaOH (h). Chemical shifts in δ/ppm.

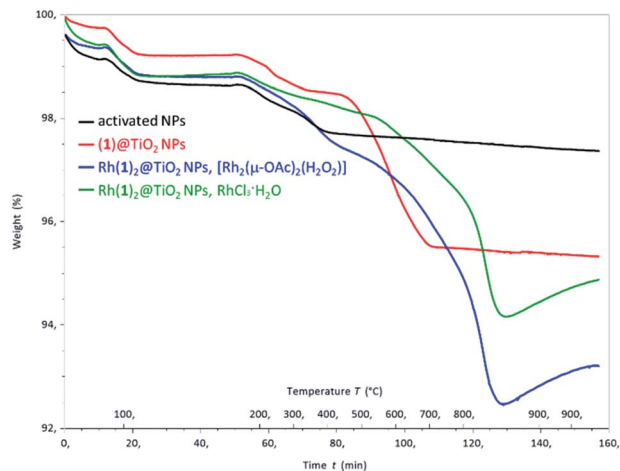


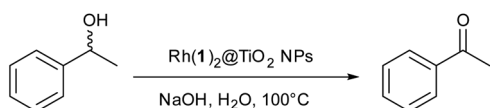
Fig. 4 TGA curves for activated NPs (black), (1)@TiO₂ NPs (red), Rh(1)₂@TiO₂ NPs made using [Rh₂(μ-OAc)₄(H₂O)₂] (blue) and for Rh(1)₂@TiO₂ NPs made using RhCl₃·3H₂O (green).

NP supported homoleptic rhodium complex for alcohol oxidation

Wang and coworkers¹² reported the dehydrogenation and aerobic oxidation of alcohols under air to produce carboxylic acids or ketones with [Rh₂Cl₂(μ-OAc)(tpy)₂]Cl as catalyst under aqueous conditions. We chose the reaction shown in Scheme 3 for a proof-of-principle investigation of the catalytic activity of Rh(1)₂@TiO₂ NPs.

For the alcohol oxidation, Rh(1)₂@TiO₂ NPs were dispersed by sonication in milliQ water. Aqueous NaOH and *rac*-(1*R*)-1-phenylethanol were added to the suspension and the mixture was again dispersed by sonication. A control (Control experiment 3) was carried out to check that NaOH (at the concentrations used in the reactions) did not strip the catalyst from the surface. The reaction was performed under air at 100 °C for 18 h, 24 h and 38 h. The product : reactant ratio was measured using ¹H NMR spectroscopy by removing a small amount of reaction solution and dispersing it in D₂O (see Experimental section). Since the reaction shown in Scheme 3 involves one reactant forming one product, it was possible to reliably determine the reactant to product ratio by comparing the peak area of the aromatic protons and the methyl protons (Fig. 5).

Control experiments (see Experimental section) were performed to investigate several key factors during the reaction. Control experiment 1 compared Rh(1)₂@TiO₂ NPs with pristine commercial NPs or activated NPs were added to the reaction vial. After the reaction, ¹H NMR spectroscopy revealed no acetophenone formation confirming that Rh(1)₂@TiO₂ NPs are the active catalyst. Control experiment 2 investigate the influence of



Scheme 3 Secondary alcohol oxidation of *rac*-(1*R*)-1-phenylethanol to acetophenone.

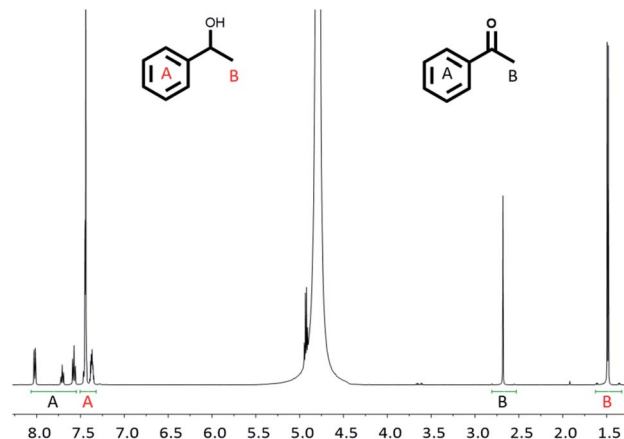


Fig. 5 ¹H NMR spectrum (500 MHz, D₂O, 298 K) of the reaction solution after alcohol oxidation (38 h) using Rh(1)₂@TiO₂ NPs as catalyst (see Experimental).

temperature with the reaction being performed at room temperature (*ca.* 22 °C) instead of 100 °C. ¹H NMR spectroscopy revealed <1% conversion to acetophenone, even after 72 h, at the lower temperature. Hence, elevated temperatures are important for product formation.

We also ensured that the reaction was catalysed by Rh(1)₂@TiO₂ NPs as opposed to [Rh(1)₂]³⁺ that had been removed from the surface. Control experiment 3 investigated if defunctionalization could occur under the basic reaction conditions. Firstly, Rh(1)₂@TiO₂ NPs and NaOH were dispersed in milliQ water. The mixture was then heated to 100 °C for 72 h to simulate the reaction conditions. Next, the NPs were separated from the solution by centrifugation, and the NPs and the supernatant solution separated into two sample vials. The substrate *rac*-(1*R*)-1-phenylethanol was added to each vial (see Experimental section) and the reaction mixtures were then heated to 100 °C for 24 h. After the reaction, ¹H NMR spectroscopy revealed no acetophenone had formed in the vial containing the supernatant solution whereas it was found in the vial containing the NPs. The results of Control 3 indicated that under the basic conditions used in the reaction, little or no defunctionalization of the NPs occurred.

Control experiment 4 investigated the influence of the concentration of the base concentration on the oxidation and allowed us to determine at what point defunctionalization occurred. Reactions were performed with NaOH – *rac*-(1*R*)-1-phenylethanol ratios of 0.01, 0.02, 0.1 and 1 (see Experimental section). Fig. 6 illustrates the reaction course of each experiment, and shows that the base concentration does not strongly influence the activity of Rh(1)₂@TiO₂ NPs with 0.01, 0.02 or 0.1 equivalents of NaOH. The catalytic activity of the Rh(1)₂@TiO₂ NPs is only affected strongly basic conditions (Fig. 6, green line).

Control experiment 5 was performed to compare the differences in catalytic activities of to [Rh(1)₂]Cl₃. We can make a number of general observations: (i) the attempt to prepare an immobilized dinuclear catalyst analogous to the established homogeneous species was unsuccessful (ii) the presence of the

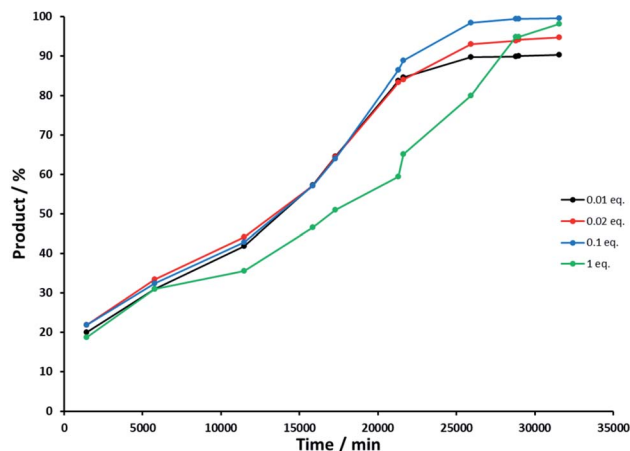


Fig. 6 Product concentration in percent against time in minutes during alcohol oxidation with varying NaOH base concentration, NaOH equivalents compared to starting material: 0.01 (black), 0.02 (red), 0.1 (blue) and 1 (green).

phosphonate functionality hinders the formation of the homogeneous dinuclear species (iii) both solution and surface chemistry leads to mononuclear complexes with **1** ligands (iv) the catalytic activity of homogeneous species depends to some extent upon the synthetic route used and (v) the catalytic activity of $\text{Rh}(\mathbf{1})_2@\text{TiO}_2$ NPs is generally similar to the homogeneous species.

Although $[\text{Rh}(\text{tpy})_2]^{m+}$ species do not appear to have been used as photocatalysts, $[\text{Rh}(\text{bpy})_3]^{m+}$ ($n = 2$ or 3) are well-established in multicomponent systems for photocatalytic reduction. We do not speculate in detail upon the mechanism of the photo-oxidation but it seems likely that the observed photooxidation product arises from the alcohol acting as a sacrificial reductant. We note that the yield of the oxidation product is somewhat reduced when the reaction is performed under argon (Table S1†). We have not observed dihydrogen production.^{40–45}

Kinetics of $\text{Rh}(\mathbf{1})_2@\text{TiO}_2$ NP catalysed alcohol oxidation

The kinetics of the alcohol oxidation by $\text{Rh}(\mathbf{1})_2@\text{TiO}_2$ NPs was investigated. The $\text{Rh}(\mathbf{1})_2@\text{TiO}_2$ NPs were dispersed in D_2O , *rac*-(1*R*)-1-phenylethanol and aqueous NaOH were added and the mixture again dispersed by sonication. The alcohol oxidation was performed under air at 100 °C for two weeks. The product – reactant ratio was determined by measuring a small amount of reaction solution dispersed in D_2O at certain time intervals with ^1H NMR spectroscopy (see Experimental section).

Analysis of the data indicated first order kinetics (Fig. 7). The data further suggested an incubation time during the first 6 h in which the reaction rate was slower. However overall *rac*-(1*R*)-1-phenylethanol was able to perform linearly over an extended period of time yielding over 71% product after the reaction.

Recyclability of $\text{Rh}(\mathbf{1})_2@\text{TiO}_2$ NPs

The recyclability of the $\text{Rh}(\mathbf{1})_2@\text{TiO}_2$ NPs was studied. In contrast to the typical procedure described earlier, the pH was monitored using a pH electrode and was returned to pH 7.8 after each cycle. The conversion of each cycle was determined from the product and starting material extracted with Et_2O from

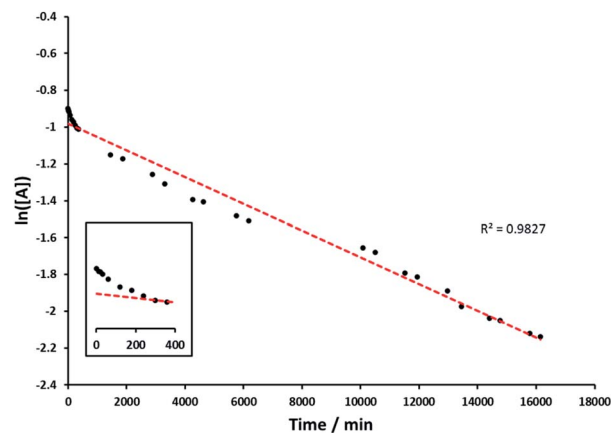


Fig. 7 1st order reaction graph, natural logarithm of starting material concentration during kinetic measurements of *rac*-(1*R*)-1-phenylethanol oxidation (see Experimental) against time in minutes (black), linear trendline through datapoints (red), insert of first 400 minutes illustrates incubation time.

the reaction solution. This had the benefits of not removing any $\text{Rh}(\mathbf{1})_2@\text{TiO}_2$ NPs from the experiment with consequent distortion of the results from the next cycle. Five reaction cycles were measured under which the conversions stayed steady at a product to reactant ratio of 1.0 : 5 (20% product) after 24 hours reaction time.

Conclusions

In this work we have built upon our previously established metal binding ligand functionalized TiO_2 NPs and use their properties to form a surface bound homoleptic rhodium complex ($\text{Rh}(\mathbf{1})_2@\text{TiO}_2$ NPs). The functionalized NPs were investigated using TGA and ^1H NMR and FT-IR spectroscopies. We further demonstrate a proof-of-principle investigation of their catalytic activity in an alcohol oxidation in water and under air. By tracking the product conversion over time with ^1H NMR spectroscopy we were able to study the reaction kinetics and the recyclability of the catalyst. $\text{Rh}(\mathbf{1})_2@\text{TiO}_2$ NPs were further compared to their non-bound counterpart concluding that the NP-bound catalyst performs similarly if not slightly better. $\text{Rh}(\mathbf{1})_2@\text{TiO}_2$ NPs were able to withstand reactions at 100 °C for at least 24 days without showing decomposition or degradation. We further studied the resistance of the functionalization to higher base concentrations. Several other control experiments were performed to exclude influencing circumstances that could lead to unintentional product formation.

Conflicts of interest

There are no conflicts to declare.

Acknowledgements

We are grateful to the Swiss National Science Foundation (grantnumber 200020_182000) and the University of Basel financial support.

Notes and references

- 1 A. Maleki, R. Taheri-Ledari, R. Ghalavand and R. Firouzi-Haji, *J. Phys. Chem. Solids*, 2020, **136**, 109200.
- 2 A. F. Hassan and H. Elhadidy, *J. Phys. Chem. Solids*, 2019, **129**, 180–187.
- 3 S. Sajjadi, A. Khataee, R. D. C. Soltani and A. Hasanzadeh, *J. Phys. Chem. Solids*, 2019, **127**, 140–150.
- 4 P. D. Stevens, J. Fan, H. M. R. Gardimalla, M. Yen and Y. Gao, *Org. Lett.*, 2005, **11**, 2085–2088.
- 5 A. Zecchina, S. Bordiga and E. Groppo, *Selective Nanocatalysts and Nanoscience*, Wiley-VHC, Weinheim, 2011.
- 6 S. Bagheri and N. M. Julkapli, *Nanocatalysts in Environmental Applications*, Springer, Cham, 2018.
- 7 S. Albonetti, R. Mazzoni and F. Cavani, in *Transition Metal Catalysis in Aerobic Alcohol Oxidation*, Royal Society of Chemistry, Cambridge, UK, 2015, ch. 1, pp. 1–39.
- 8 M. Bartz, J. Küther, R. Seshadri and W. Tremel, *Angew. Chem., Int. Ed.*, 1998, **37**, 2466.
- 9 S. Ali, M. J. Al-Marri, A. G. Abdelmoneim, A. Kumar and M. M. Khader, *Int. J. Hydrogen Energy*, 2016, **41**, 22876–22885.
- 10 H. Göksu, H. Burhan, S. D. Mustafafov and F. Şen, *Sci. Rep.*, 2020, **10**, 5439.
- 11 S. A. Freimann, D. Zare, C. E. Housecroft and E. C. Constable, *Nanoscale Adv.*, 2020, **2**, 679–690.
- 12 X. Wang, C. Wang, Y. Liu and J. Xiao, *Green Chem.*, 2016, **18**, 4605.
- 13 V. Spampinato, N. Tuccitto, S. Quici, V. Calabrese, G. Marletta, A. Torrisi and A. Liccardello, *Langmuir*, 2010, **26**, 8400.
- 14 <https://www.aerosil.com/sites/lists/RE/DocumentsSI/TI-1243-Titanium-Dioxide-as-Photocatalyst-EN.pdf>, (accessed 05 April 2020).
- 15 J. Paul, S. Spey, H. Adams and J. A. Thomas, *Inorg. Chim. Acta*, 2004, **357**, 2827.
- 16 *Software for the Integration of CCD Detector System Bruker Analytical X-ray Systems*, Bruker axs, Madison, WI (after 2013).
- 17 G. M. Sheldrick, *Acta Crystallogr., Sect. A: Found. Adv.*, 2015, **71**, 3.
- 18 O. V. Dolomanov, L. J. Bourhis, R. J. Gildea, J. A. K. Howard and H. Puschmann, *J. Appl. Crystallogr.*, 2009, **42**, 339.
- 19 G. M. Sheldrick, *Acta Crystallogr., Sect. C: Struct. Chem.*, 2015, **27**, 3.
- 20 C. F. Macrae, I. Sovago, S. J. Cottrell, P. T. A. Galek, P. McCabe, E. Pidcock, M. Platings, G. P. Shields, J. S. Stevens, M. Towler and P. A. Wood, *J. Appl. Crystallogr.*, 2020, **53**, 226.
- 21 E. C. Constable, *Adv. Inorg. Chem.*, 1986, **30**, 69–121.
- 22 C. Wei, Y. He, X. Shi and Z. Song, *Coord. Chem. Rev.*, 2019, **385**, 1–19.
- 23 R. Calzada, C. M. Thompson, D. E. Westmoreland, K. Edme and E. A. Weiss, *Chem. Mater.*, 2016, **28**, 6716.
- 24 J. De Roo, K. De Keukeleere, Z. Hens and I. Van Driessche, *Dalton Trans.*, 2016, **45**, 13277.
- 25 J. De Roo, Z. Zhou, J. Wang, L. Deblock, A. J. Crosby, J. S. Owen and S. S. Nonnenmann, *Chem. Mater.*, 2018, **30**, 8034.
- 26 L. Du, W. Wang, C. Zhang, Z. Jin, G. Palui and H. Mattoussi, *Chem. Mater.*, 2018, **30**, 7269.
- 27 C. Goldmann, F. Ribot, L. F. Peiretti, P. Quaino, F. Tielens, C. Sanchez, C. Chanéac and D. Portehault, *Small*, 2017, **13**, 1604028.
- 28 V. Grigel, L. K. Sagar, K. De Nolf, Q. Zhao, A. Vantomme, J. De Roo, I. Infante and Z. Hens, *Chem. Mater.*, 2018, **30**, 7637.
- 29 M. L. Kessler, H. E. Starr, R. R. Knauf, K. J. Rountree and J. L. Dempsey, *Phys. Chem. Chem. Phys.*, 2018, **20**, 23649.
- 30 R. R. Knauf, J. C. Lennox and J. L. Dempsey, *Chem. Mater.*, 2016, **28**, 4762.
- 31 M. La Rosa, T. Avellini, C. Lincheneau, S. Silvi, I. A. Wright, E. C. Constable and A. Credi, *Eur. J. Inorg. Chem.*, 2017, **2017**, 5143.
- 32 A. Ritchhart and B. M. Cossairt, *Inorg. Chem.*, 2019, **58**, 2840.
- 33 C. M. Harris and E. D. McKenzie, *J. Inorg. Nucl. Chem.*, 1963, **25**, 171–174.
- 34 E. Botha, M. Landman, P. H. van Rooyen and E. Erasmus, *Inorg. Chim. Acta*, 2018, **482**, 514–521.
- 35 B. Kim, S. W. Park, J.-Y. Kim, K. Yoo, J. A. Lee, M.-W. Lee, D.-K. Lee, J. Y. Kim, B. S. Kim, H. Kim, S. Han, H. J. Son and M. J. Ko, *ACS Appl. Mater. Interfaces*, 2013, **5**, 5201.
- 36 See for example: A. Estrada-Monje, R. Zitzumbo-Guzmán, J. A. Bañuelos-Díaz and E. A. Zaragoza-Contreras, *Mater. Chem. Phys.*, 2019, **235**, 121760.
- 37 See for example: M. Nilsing, S. Lunell, P. Persson and L. Ojamäe, *Surf. Sci.*, 2005, **582**, 49; C. Queffélec, M. Petit, P. Janvier, D. A. Knight and B. Bujoli, *Chem. Rev.*, 2012, **112**, 3777.
- 38 V. Spampinato, N. Tuccitto, S. Quici, V. Calabrese, G. Marletta, A. Torrisi and A. Liccardello, *Langmuir*, 2010, **26**, 8400.
- 39 A. J. Stephens, F. J. Malzner, E. C. Constable and C. E. Housecroft, *Sustainable Energy Fuels*, 2018, **2**, 786.
- 40 M. Kirch, J. M. Lehn and J. P. Sauvage, *Helv. Chim. Acta*, 1979, **62**, 1345.
- 41 B. Hubsch and B. Mahieu, *Polyhedron*, 1985, **4**, 669.
- 42 B. Hubsch, B. Mahieu and J. Meunier-Piret, *Bull. Soc. Chim. Belg.*, 1985, **94**, 685.
- 43 H. Hukkanen and T. T. Pakkanen, *J. Mol. Catal.*, 1986, **37**, 297.
- 44 V. E. Maier and V. Y. Shafirovich, *Kinet. Katal.*, 1987, **28**, 839.
- 45 Y. Kataoka, K. Sato, Y. Miyazaki, Y. Suzuki, H. Tanaka, Y. Kitagawa, T. Kawakami, M. Okumura and W. Mori, *Chem. Lett.*, 2010, **39**, 358.